Polymer Degradation and Stability 244 (2026) 111792

Contents lists available at ScienceDirect

Polymer Degradation and Stability

journal homepage: www.journals.elsevier.com/polymer-degradation-and-stability

Ecofriendly synthetic strategies for the realization of FDCA-based polymer films for sustainable, flexible and recyclable/compostable food packaging

Giulia Guidotti [a], Michelina Soccio [a,b,c,*], Valentina Siracusa [d], Elisabetta Salatelli [e], Nadia Lotti [a,b,f]

[a] Department of Civil, Chemical, Environmental and Materials Engineering, University of Bologna, Via Terracini 28, Bologna 40131, Italy
[b] Interdepartmental Center for Industrial Research on Advanced Applications in Mechanical Engineering and Materials Technology, CIRI-MAM, Viale del Risorgimento 2, Bologna 40136, Italy
[c] Interdepartmental Center for Industrial Research on Buildings and Construction CIRI-EC, Via del Lazzaretto 15/5, Bologna 40131, Italy
[d] Department of Chemical Science, University of Catania, Viale A. Doria 6, Catania 95125, Italy
[e] Department of Industrial Chemistry "Toso Montanari", University of Bologna, Viale Risorgimento 4, Bologna 40136, Italy
[f] Interdepartmental Center for Industrial Agro-Food Research, CIRI-AGRO, Via Quinto Bucci 336, Cesena 47521, Italy

ARTICLE INFO

Keywords:
2,5-furandicarboxylic acid
Poly(octylene 2,5-furanoate)
Poly(triethylene 2,5-furanoate)
Copolymers
Mechanical properties
Gas barrier
Compostability
Food packaging

ABSTRACT

Novel 2,5-furandicarboxylic acid-based polyesters, by combining poly(octylene 2,5-furanoate) and poly(triethylene 2,5-furanoate), were successfully synthesized, characterized and evaluated for sustainable and flexible food packaging application. Three eco-friendly and solvent-free synthetic approaches, such as melt polycondensation, physical blending and reactive blending were employed to prepare: equimolar physical blend, 50 mol% of poly(octylene 2,5-furanoate) block and random copolymers, 80 mol% of poly(octylene 2,5-furanoate) random copolymer.

After molecular characterization, by nuclear magnetic resonance spectroscopy and gel permeation chromatography, confirming the good control of synthesis parameters, the polymers were processed in form of films and subjected to solid-state properties characterization.

High thermal stability was evidenced by thermogravimetric analysis, while the characteristic temperatures were determined through differential scanning calorimetry showing all the polymers, with the exception of poly(triethylene 2,5-furanoate), are capable of developing ordered structures. Diffractometric measurements showed poly(octylene 2,5-furanoate) crystals, in comparable amount but with different perfections degree, formed in all the crystalline samples.

Scanning electron microscopy was employed to assess film microstructure, distribution and continuity.

Functional properties, such as mechanical behavior and gas barrier capability, were tested and correlated with chemical, structural/microstructural and thermal characteristics of the polymer films.

Surface wettability was measured and correlated with the composting ability and kinetics.

In general, flexibility was enhanced while keeping the gas barrier ability even under humid conditions, while degradation rate in compost was properly tuned in the perspective of different end of life management of the polymer films.

1. Introduction

The use of plastics and the consequent environmental impact is undoubtedly one of the most discussed topics in the current century. Plastic littering is affecting our marine and terrestrial environment, with devastating consequences for natural habitat biodiversity and ecosystems, impacting also human activities and health [1,2] It has been estimated that the volume of waste production is of about 2–2.5 kg/day per capita in developed countries and about 0.5–1 kg/day per capita in the other countries [3] Luckily, society and politics are becoming more aware about the plastics environmental impact issue, and governments introduced and continuously update policies aiming to reduce plastics use in a systemic way [4,5] For example, the Osaka Blue Ocean Vision program is pushing G20 countries to reduce additional pollution by

* Corresponding author.
E-mail address: m.soccio@unibo.it (M. Soccio).

https://doi.org/10.1016/j.polymdegradstab.2025.111792
Received 26 September 2025; Received in revised form 15 November 2025; Accepted 18 November 2025
Available online 19 November 2025

marine plastic litter to zero by 2050, making the net volume of plastics entering the ocean zero by that time [6,7] Moreover, the European Union (EU) adopted a strategy for plastics as part of the EU's circular economy action plan, aiming to support a more sustainable and safer consumption and production patterns for plastics, differently from the dominant linear economic development model, based on "take, make and dispose" [8] Another Directive of the EU was introduced on waste landfills to reduce the volumes of disposed waste and set strict requirements for landfilling [9] As a result, positive signals have come: from 2006 recycling has become the first option for plastics wastes in Europe, with an increase rate of 117 % between 2006 and 2020 [10] Despite all the measures taken, still 23 % of plastics wastes are discharged in landfills in Europe, [10] while in the middle and lower-income countries, this is even the first option, open dumping and open burning treatments being largely preferred [11,12]

On the other hand, it is commonly accepted that plastic materials play a central role in everyday life: it has been estimated that more than 8300 million metric tons of virgin plastics have been produced to date, [13] and their global market, which was of about 609 billion dollars in 2022, is estimated to further grow at a CAGR of 4.0 % from 2023 to 2030 [14] As known, the success of plastics is related to their low cost, high availability, light-weight and the possibility to easily tune their functional properties according to the intended uses. Among these last, packaging, including food one, is for sure the most important application, covering alone almost the 40 % of plastics market [15] Being impossible to think a world without plastics, sustainable solutions must be found. The first action is the replacement of traditional rigid packages with flexible ones. This way, plastic volumes could be drastically reduced, minimizing wastes and preserving sources and energy during production and transport [16] It has to be emphasized that, in the case of food packaging, barrier performances to external environment, in particular to moisture and oxygen, are preserved or even improved by using flexible packages, with consequent prolonged food shelf-life and reduced food waste, the other plague of our century [17] A second solution is recycling of plastic wastes, although recycling is not always practicable, because of package contamination by organic matter and multilayer nature of most of the plastic materials present in the market of food packaging [18] These problems could be overcome by using mono-material packaging that, of course, must be characterized by suitable mechanical and barrier properties as multi-material packaging. Equally important would be the use of renewable sources, such as biomass and agro-food wastes for plastics production, instead of fossil ones. In this regard, the US Department of energy provided a list of top value-added chemicals obtainable from biomass. 2,5-furandicarboxylic acid (FDCA) is the only bio-based aromatic chemical among the 12 most important ones [19] Accordingly, furan-based polyesters have become research hotspot in recent years and can be considered among the materials of the future, [20–22] since they respond positively to the various actions undertaken to reduce the environmental impact caused by plastics, showing excellent mechanical and barrier properties, some of them being also biodegradable or compostable [23–27]

In the present work, the Authors focused their attention on two furan-based polyesters, nominally poly(octylene 2,5-furanoate) (POF) and poly(triethylene 2,5-furanoate) (PTEF). The two homopolymers have similar repeating unit, triethylene glycol differing from 1,8-octanediol only for the presence of two ether oxygen atoms instead of two -CH_2- groups in position 3 and 6 of the aliphatic moiety. To the best of our knowledge, PTEF has been never synthesized and studied before, whereas some papers are present in the literature on POF, [28,29] although none of these mention its mechanical response, gas barrier properties or compostability. As already evidenced for other polymeric systems, [30–33] the presence of -C-O—-C- ether bonds along the macromolecular chain affect crystallizing ability, surface hydrophobicity and rigidity, reducing all of them. The introduction of ether oxygen atoms, in turn, influence water affinity and, consequently, hydrolytic and enzymatic degradation. To obtain new polymer materials with finely tunable properties, the two POF and PTEF homopolymers have been combined both physically, by blending, and chemically, by copolymerization. Through these approaches it was possible to obtain a physical blend, block copolymers with different block length, keeping fix the chemical composition (50 mol % OF), and a random copolymer with different composition (80 mol % OF). All the materials were processed into free-standing films by compression moulding. Beside molecular and thermal characterization, mechanical response and barrier properties to dry as well as humid O_2 and CO_2 gases were also evaluated, to check the suitability of the new materials for flexible food packaging purposes. Lastly, lab scale composting experiments were carried out to evaluate their possible use as recyclable mono-material films or biodegradable devices.

2. Experimental section

2.1. Materials

Dimethyl furanoate (DMF) was purchased from Sarchem Labs, while 1,8-octanediol (OD), triethylene glycol (TEG), titanium tetrabutoxide (TBT) and titanium isopropoxide (TIP) were purchased from Merck and used reagent-grade.

2.2. Homopolymers synthesis

Poly(octylene furanoate) (POF) and poly(triethylene furanoate) (PTEF) were synthesized through two-step melt polycondensation technique. The synthetic apparatus was composed by a glass reactor, put in a thermostated silicon oil bath, a mechanical stirrer connected to a torque measurer and a high vacuum pump. A mixture of two catalysts, TBT and TIP, was used (200 ppm each). A glycol excess of 30 mol %, was employed. During the first synthetic phase, the temperature was set at 190 °C and the reaction was carried out under inert N_2 atmosphere for 90 min after monomer dissolution, with a continuous stirring of 100 rpm. During this step, transesterification reactions occured, together with distillation of methanol. At the beginning of the second phase, which lasted about 180 min, the pressure was gradually reduced to 0.05 mbar and the temperature was raised to 230 °C. During this step, polycondensation reactions took place, the glycol released was collected in a trap: a raise of torque value, due to the increase of polymeric fluid viscosity, i.e. of molecular weight, could be observed. When torque reached a plateau value, the synthesis was stopped, and the polymers were discharged from the reactor.

2.3. Chemical modification strategies

Chemical modification of POF and PTEF homopolymers was carried out by three different strategies: melt copolymerization, physical and reactive blending (Scheme 1). More in detail, the same polycondensation procedure used for the synthesis of the two homopolymers was adopted also for the synthesis of the random copolymer poly (octylene/triethylene furanoate) P(O_{80}/TE_{20}F) containing 80 mol % OF.

An equimolar physical blend (POF_{50}/$PTEF_{50}$) was prepared by dissolving and mixing the two homopolymers in $CHCl_3$. Afterwards, chloroform was evaporated.

Two different poly(octylene/triethylene furanoate) copolymers, characterized by the same chemical composition (50 mol % OF) but a different molecular architecture, were obtained by reactive blending the previous prepared POF_{50}/$PTEF_{50}$ physical mixture, for 15 and 45 min, respectively, in a 250 mL glass reactor under nitrogen flow and continuous stirring (100 rpm), keeping the temperature at 225 °C. Copolymer formation was catalysed by TBT and TIP already present in the homopolymers. Different mixing times allowed to obtain copolymers with long and short blocks, P(O_{50}-*b*-TE_{50}F) and P(O_{50}/TE_{50}F), respectively.

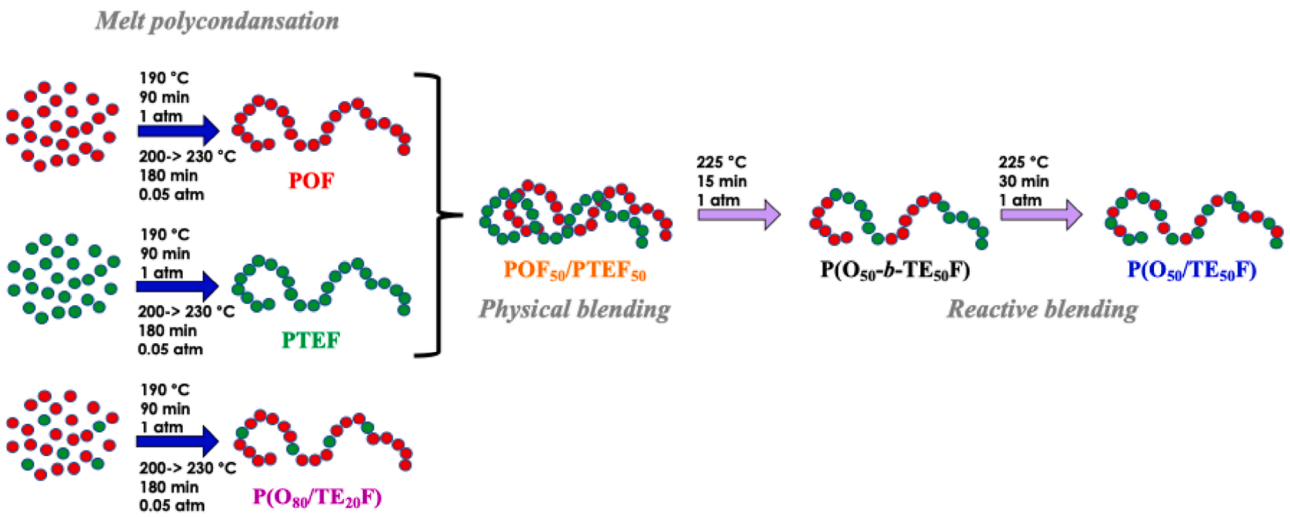

Scheme 1. Summary of the different synthetic strategies adopted in the present work: melt polycondensation; physical blending; reactive blending.

2.4. Molecular characterization

The chemical structure and the composition were determined by proton Nuclear Magnetic Resonance (^{1}H-NMR), while the degree of randomness (b) and the block length were calculated by means of carbon Nuclear Magnetic Resonance (^{13}C-NMR). The solutions were prepared by solving the polymers in deuterated chloroform (containing tetramethylsilane as internal standard) with a concentration of 10mg/mL for samples analyzed by ^{1}H-NMR , and of 40 mg/mL for samples analyzed by ^{13}C-NMR . A Varian INOVA 400 MHz apparatus, operating at room temperature, was employed.

Molecular weight (M_n) and polydispersity index ($Đ$) were determined through gel permeation chromatography (GPC), carried out at 30 °C. The apparatus is formed by a 1525 binary HPLC pump (Waters) equipped with PLgel 5 mm MiniMIX-C column (Agilent Technologies) and a refractive index detector, calibrated using monodisperse polystyrene standards in the range of 2000–100,000 Da. Samples were solved in chloroform, which was used also as eluent (flow of 1 mL/min).

2.5. Film preparation

Polymeric films (of about 100 μm thickness) were obtained by compression molding, using a Carver C12 Laboratory press, equipped with a water cooling apparatus. About 2 g of material were placed between two Teflon sheets and melted in the press. After that, a pressure of about 6 ton/m^2 was applied for two minutes and films were then cooled to room temperature in the press. Before further characterization, all the polymeric films were stored at room temperature for three weeks, in order to let them reach thermal equilibrium.

2.6. Surface characterization

Static contact angle measurements were carried out on film samples by using a KSV CAM101 instrument (Helsinki, Finland) at room temperature, recording the profiles of water drops by image analysis (tangent method 1). Each drop (4μl) was deposited at a rate of 100 μl/min on the film surface. At least ten drops were observed on different areas for each film and contact angles were reported as the average value ± standard deviation. The data were also recorded at different times after deposition (30 s, 60 s), in order to evaluate the evolution of the drop shape and the value of WCA.

2.7. Thermal and structural characterization

Thermal stability was determined by thermogravimetric analysis (TGA), using a TGA4000 (Perkin Elmer) instrument. About 5 mg of each polymeric samples were loaded on a weight scale and heated under N_2 flow at a rate of 10 °C/min in the temperature range 40–800 °C. By this technique it was possible to measure T_{onset} and T_{max}, i.e. the temperature at which weight loss starts and the temperature corresponding to maximum weight loss, respectively.

Polymer films' thermal transitions were determined with differential scanning calorimetry (DSC), by means of a DSC6 (Perkin Elmer) instrument. This last is composed by an intracooler set at −70 °C and a holder, containing both the sample and the reference, kept under N_2 atmosphere. The samples were subjected to the following calorimetric program: I heating scan from −40 °C to 190 °C (rate of 20 °C/min), an isothermal step of 3 min, a rapid cooling from the molten state, by immersion in liquid nitrogen, and then a II heating scan, under the same conditions of the I scan. Thermal transitions like glass to rubber transition temperature (T_g), crystallization temperature (T_{cc}) and melting temperature (T_m) as well as their relative specific heat and enthalpy variations (Δc_p, ΔH_{cc} and ΔH_m, respectively) were calculated.

The kind and amount of crystalline phase developed by the films investigated were determined by means of wide-angle X-Ray scattering (WAXS), using a with a PANalytical X'Pert PRO diffractometer equipped with an X'Celerator detector and a copper target. Data were acquired at room temperature in the 5–60° 2θ range (acquisition time of 100 s; step of 0.10°). Crystallinity degree (X_c) was calculated as the ratio between the area related to the crystalline peaks and the overall area under the diffractometric curve. The non-coherent scattering was also considered.

Scherrer equation was applied for domain size determination [34]

2.8. Mechanical characterization

Mechanical response of the polymeric samples was tested using an Instron 5966 machine, equipped with rubber grips, a 10 kN load cell and a Bluehill software. Each rectangular film (5 mm × 50 mm, gauge length of 20 mm) was subjected to stress-strain measurements, by applying a stretching speed of 10 mm/min. The load-displacement data directly measured by the instrument have been converted to stress−strain curves by the software. Stress (σ_B) and elongation (ε_B) at break were directly calculated, while the tensile elastic modulus (E) was determined from the initial linear slope of each curve. At least 6 samples for each material were analyzed, and the mean value ± standard deviation of the 6 measurements was reported.

2.9. Barrier properties evaluation

Permeability tests were performed at room temperature (23 °C) using a Permeance Testing Device, type GDP-C (Brugger Feinmechanik GmbH), using a manometric method. The sample temperature was regulated by an external thermostat HAAKE-Circulator DC10-K15 type (Thermoscientific, Selangur Darul Ehnsan, Malaysia). Each polymeric film (area of 78.5 cm^2, diameter of 10 cm) has been placed between two chambers, the upper one then filled with the test gas (O_2 and CO_2) at a pressure of 1 atm and a stream of 100 cm^3min^{-1}. A pressure transducer, placed in the lower chamber, measures the increasing of gas pressure as a function of time. From pressure/time plot, the software calculates permeation, which can be converted in permeability. The gas transmission rate (GTR), i.e. the value of the film permeability to gas, was determined considering the increase in pressure in relation to the time and the volume of the device. Two different relative humidity (RH) values were considered, 0 % RH and 85 % RH, in order to mimic both dry and humid conditions. All the measurements have been performed at least in triplicate, and the mean value ± standard deviation was reported.

2.10. Compostability evaluation

Lab-scale compostability tests were performed by placing polymeric square films (15 × 15 mm^2), previously weighted, in between two layers of mature wet compost, kindly supplied by Nuova Geovis (Sant'Agata Bolognese, Italy). Samples were incubated at 58 °C and 99 % RH, under agitation (50 rpm) using a SW22 Julabo shaking water bath. At designed time points, specimen duplicates were withdrawn, washed repeatedly with an aqueous solution of ethanol (70 % v/v) and then dried until constant weight was reached. Gravimetric weight loss was determined dividing the difference between initial and final weight of each sample by the initial one.

Surface morphology of partially degraded samples was observed with a Hitachi S-2400 scanning electron microscope (SEM) operating at 18 kV. Before the analysis, samples were glued on aluminum stabs with carbon tape and gold sputtered. Molecular and thermal characterization were carried out on partially degraded samples in order to check differences in chemical composition and in thermal transitions ascribable to degradation process.

3. Results and discussion

In the present study, a physical blend and several copolymers of POF and PTEF were obtained. The two homopolymers are characterized by very similar chemical structure, differing just for the presence of two ether oxygen atoms instead of two CH_2 groups in the glycolic subunit. We have evaluated: i) the effect of physical and chemical blending (physical mixture vs. copolymer) keeping fixed the composition (50:50, OF mol:TEF mol); ii) the effect of molecular architecture (block vs. random copolymer) keeping fixed the composition (50:50, OF mol:TEF mol); iii) the effect of chemical composition (80:20 vs. 50:50, OF mol:TEF mol), keeping fixed the molecular architecture (random).

3.1. Synthesis and molecular characterization

POF and PTEF homopolymers and random P(O_{80}/TE_{20}F) copolymer were synthesized by two-step melt polycondensation using TBT and TIP as catalysts. The POF_{50}/$PTEF_{50}$ physical blend was prepared through the solution of equimolar amount of POF and PTEF in chloroform under stirring, and further evaporation of the solvent. Block P(O_{50}-*b*-TE_{50}F) and random P(O_{50}/TE_{50}F) copolymers were synthesized by reactive blending the homopolymers physical blend. The as-prepared samples were firstly characterized from the molecular point of view by means of ^{1}H-NMR and ^{13}C-NMR spectroscopy and GPC analysis. By ^{1}H-NMR it was possible to confirm the chemical structure and to calculate the chemical composition. The molecular characterization data are collected in Table 1, while in Fig. 1A, ^{1}H-NMR spectrum of P(O_{50}-*b*-TE_{50}F) is reported as an example, together with peaks' assignment. At low field, close to the chloroform signal, the peaks related to the aromatic furan ring (*a* and *a'* protons) can be detected at 7.23 and 7.24 ppm. In the region between 1.25 and 4.50 ppm, the characteristic signals of the glycol subunits can be observed. In detail, the peaks of the methylene groups in α position to the ester oxygen are present: *b* at 4.30 ppm related to octylene and *f* at 4.45 ppm of triethylene, respectively. The remaining protons are located at higher field: the *d* and *e* signals of hydrogen atoms of the octylene moiety are overlapped and located at 1.35 ppm, while the *g* and *h* protons of triethylene subunit are located at 3.81 and 3.68 ppm, respectively.

The actual chemical composition was calculated from the relative area of *f* methylene protons of TEG subunit at δ 4.45 ppm, and the relative area of *b* protons of OD at δ 4.30 ppm. For all the materials under investigation, the molar amount of TEF turned out to be very close to the feed one (Table 1).

^{13}C-NMR analysis was used to determine block length (L) and randomness degree (b). In Fig. 2 the ^{13}C-NMR spectrum of P(O_{50}-*b*-TE_{50}F) block copolymer with peaks' assignment is shown as an example. A magnification of the spectra of the two parent homopolymers together with those of P(O_{50}-*b*-TE_{50}F) and P(O_{50}/TE_{50}F) copolymers in the range 146.2 - 147.4 ppm, is also shown. In this region, together with the signals at 146.91 and 146.70 ppm, corresponding to the O-F-O (*j* carbon) and TE-F-TE (*j'* carbon) triads, respectively, two additional peaks can be detected. These signals (*w* and *y*) refer to the O-F-TE and TE-F-O triads. The signals due to ester group carbons, *i* and *i'*, can be also detected in the range 157.90–158.20 ppm, while *k* and *k'* peaks are located between 118.1 and 118.7 ppm. In addition, the signals of glycol carbons of octylene subunit (*l, m, n* and *o*) appeared at 65.75, 29.00, 25.60 and 28.25 ppm, respectively, while the carbons of triethylene subunit (*p, q* and *r*) were located at 64.50, 68.90 and 70.70 ppm, respectively.

As to the degree of randomness (b), it must be noted that it is equal to 1 for random copolymers, 2 for alternate copolymers, 0 for a mixture of two corresponding homopolymers and $0 < b < 1$ for block copolymers. In the present work, the degree of randomness was calculated according to Eq. (1):

$$b = P_{O\text{-}TE} + P_{TE\text{-}O} \quad (1)$$

where O-TE and TE-O are the probability of finding an O unit next to a TE one and the probability of finding a TE next to an O one, respectively.

These two probabilities can be expressed, in turn, according to Eq. (2) and 2′:

$$P_{O-TE} = \frac{I_w}{I_j + I_w}; \; P_{TE-O} = \frac{I_y}{I_{j'} + I_y} \quad (2)$$

where, I_w, I_j, I_y, I_j, represent the integrated intensities of *w, j, y* and *j'* resonance peaks related to the O-F-TE, O-F-O, TE-F-O, and TE-F-TE triads, respectively (Fig. 2).

For P(O_{80}/TE_{20}F) and P(O_{50}/TE_{50}F) copolymers, the calculated b is practically equal to 1, while for P(O_{50}-*b*-TE_{50}F) copolymer b was 0.21, in agreement with their predicted molecular architecture.

The average length (L) of OF and TEF sequences is reported in

Table 1
Molecular characterization data (NMR and GPC) of the materials under investigation.

	TEF mol %	L_{OF}	L_{TEF}	*b*	M_n g/mol	*Đ*
POF	-	-	-	-	34,700	2.4
POF_{50}/$PTEF_{50}$	50	-	-	-	-	-
P(O_{50}-*b*-TE_{50}F)	49	11.1	10.1	0.21	26,400	2.1
P(O_{50}/TE_{50}F)	49	2.3	2.1	0.98	40,700	2.1
P(O_{80}/TE_{20}F)	19	5.0	1.1	1.00	32,400	2.2
PTEF	100	-	-	-	26,700	2.0

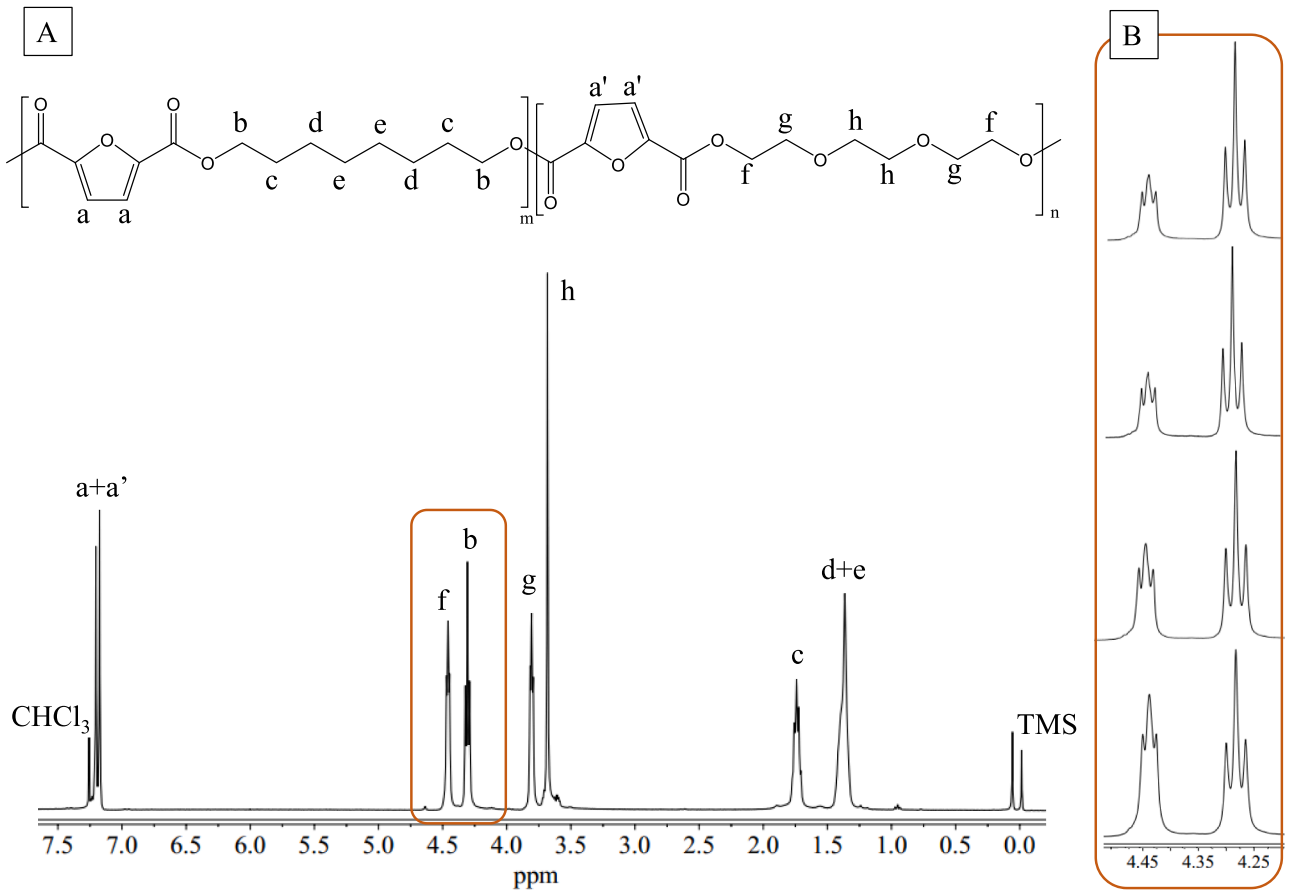

Fig. 1. A) ^{1}H-NMR spectrum of P(O_{50}-*b*-TE_{50}F) copolymer with peaks' assignment; B) Magnification of the region between 4.25 and 4.55 ppm of the ^{1}H-NMR spectra of neat (bottom) and partially degraded (moving to top) P(O_{50}-*b*-TE_{50}F) samples.

Table 1 and was calculated according to Eq. (3) and 3′:

$$L_{OF} = \frac{1}{P_{O-TE}};\ L_{TEF} = \frac{1}{P_{TE-O}} \quad (3)$$

As expected, P(O_{80}/TE_{20}F) is characterized by L_{TEF} equal to 1.1 and L_{OF} equal to 5.0, due to the presence of a higher amount of OF subunits with respect to TEF ones, as a consequence of its chemical composition. In the case of the two copolymers obtained by reactive blending, by increasing the mixing time, the average block length decreased (from 11.1 and 10.1 to 2.3 and 2.1), confirming the proceeding of trans-esterification reactions and the evolution from a block architecture (P(O_{50}-*b*-TE_{50}F)) to a random one (P(O_{50}/TE_{50}F)). Molecular weight obtained by GPC (Table 1) were high and comparable, all characterized by a quite low polydispersity index (ranging from 2.0 to 2.4), suggesting a good control over the syntheses.

3.2. Thermal and structural characterization

The compression molded films were subjected to calorimetric studies after three weeks of storage at room temperature, in order to uniform their thermal history, being all the polymers under study characterized by a T_g below room temperature. Thermal stability was measured by means of thermogravimetric analysis under N_2 flow. The relative thermograms are shown in Fig. 3aA, while in Table 2, the temperatures corresponding to initial decomposition (T_{onset}) and to maximum degradation rate (T_{max}) are listed. All the polyesters investigated are high thermally stable, with T_{onset} above 360 °C, in agreement with results previously obtained on other furan-based polyesters [36,37] PTEF is the polymer that starts degrading at lowest temperature, due to the presence of ether oxygen atoms along its macromolecular chain, which are the first involved during thermal degradation [36] Conversely, POF has a T_{onset} of 379 °C. As to the T_{max} values, the differences between the two homopolymers are less pronounced, due to the fact that at this stage, degradation occurs in both OF and TEF moieties. All the copolymers and the blend have an intermediate behaviour for both values, confirming that copolymerization did not worsen the thermal stability, on the contrary, as reactive blending time increases T_{max} also increases (for P(O_{50}/TE_{50}F) random copolymer). In all cases, no char residue was observed and degradation occurred in two different steps, the second and less remarked one at higher temperatures (around 500 °C).

Thermal transitions were measured by DSC analysis, which was carried out on all the samples in form of compression moulded films. The relative calorimetric data are collected in Table 2, while the I scan DSC trace is shown in Fig. 3B In the I scan, POF shows the typical behavior of semicrystalline materials, with a glass transition phenomenon followed by an endothermic melting peak at higher temperature (145 °C). Conversely, PTEF is completely amorphous, only the endothermic baseline deviation related to glass-to-rubber transition (11 °C) being present. The copolymers and blend are all semicrystalline materials, with melting temperatures and enthalpy values changing as a function of TEF amount and molecular architecture. More in detail, POF_{50}/$PTEF_{50}$ blend is characterized by the same T_m value of POF, with a halved value of ΔH_m, in agreement with the amount, inside the blend of POF, which is the only polymer able to crystallize. P(O_{50}-*b*-TE_{50}F) block copolymer has lower T_m (136 °C vs. 145 °C for POF) and ΔH_m (21 J/g vs. 41 J/g for POF), confirming the multi-block nature of the copolymer. The enthalpy variation halving is in agreement with the chemical composition (Table 1), i.e. the reduction of the crystallisable OF segments per unit mass.

If P(O_{50}/TE_{50}F) and P(O_{50}-*b*-TE_{50}F) are compared, T_m decreased

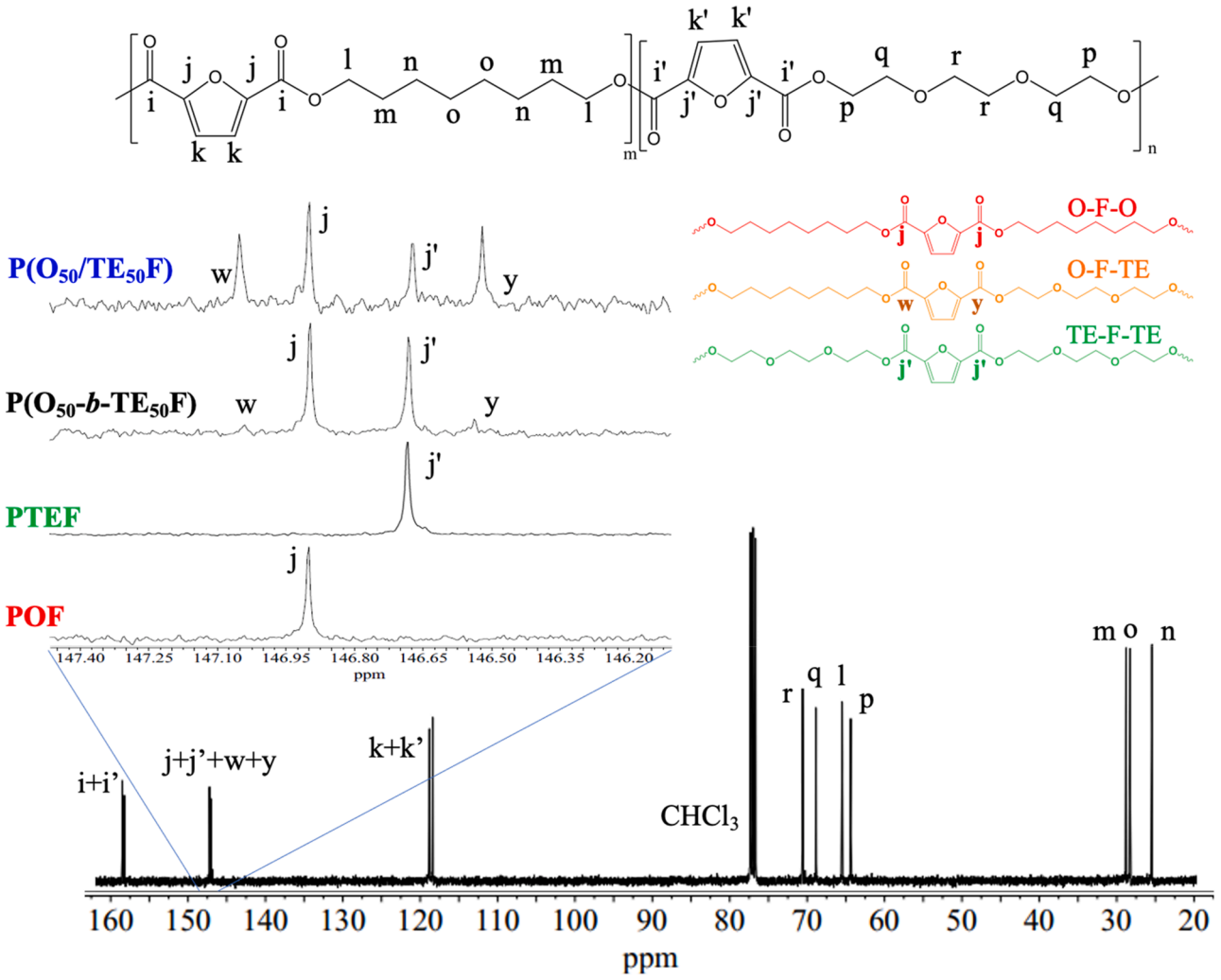

Fig. 2. ^{13}C-NMR spectrum of P(O_{50}-*b*-TE_{50}F) block copolymer with peaks' assignment. In the inset, a magnification of the spectra of POF, PTEF, P(O_{50}-*b*-TE_{50}F) and P(O_{50}/TE_{50}F) in the region between 146.2 and 147.4 ppm is reported.

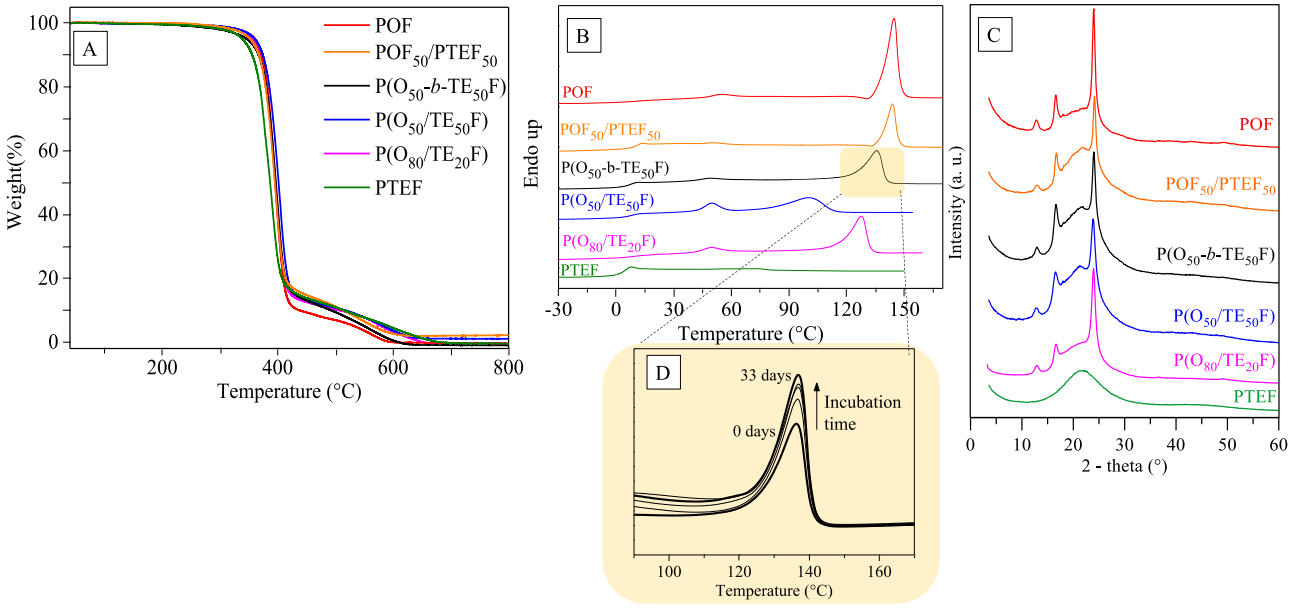

Fig. 3. A) Thermograms obtained by TGA; B) I scan DSC curves; C) WAXS profiles of the materials under investigation and D) Magnification of the region corresponding to the melting temperature (90–170 °C) of DSC curves of partially degraded P(O_{50}-*b*-TE_{50}F) samples.

Table 2
Thermal (TGA and DSC) and structural (WAXS) characterization data of the materials under investigation.

	T_{onset}°C	T_{max}°C	I scan				II scan						X_c%	$\hat{L}$ nm
			T_g°C	ΔC_p J/g°C	T_m°C	ΔH_m J/g	T_g°C	ΔC_p J/g°C	T_{cc}°C	ΔH_{cc} J/g	T_m°C	ΔH_m J/g		
POF	379	396	18	0.157	54, 145	2.5 41	−2	0.284	18	19	144	48	37	14
$POF_{50}/PTEF_{50}$	374	395	10	0.332	144	20	−2 7	0.234 0.008	17	7	143	22	18	14
$P(O_{50}$-*b*-$TE_{50}F)$	374	399	6	0.292	49, 136	2.2 21	1	0.302	30	18	136	25	18	12
$P(O_{50}/TE_{50}F)$	379	403	8	0.316	50, 100	5.4 22	3	0.381	66	16	102	16	19	9
$P(O_{80}/TE_{20}F)$	374	397	11	0.177	49, 128	3.4 29	1	0.162	31	28	127	37	28	10
PTEF	361	390	11	0.587	-	-	11	0.505	-	-	-	-	-	-

ˆ Mean domain size estimated by the width of the peak at 24° in the WAXS pattern.

with block length, indicating a reduction of crystal perfection and dimension, as also confirmed by the broad shape of the melting phenomenon. The comparable values of ΔH_m indicate that, although particularly disturbed by the presence of TEF segments, OF short blocks are still able to crystallize.

$P(O_{80}/TE_{20}F)$ shows values of both T_m and ΔH_m in between those of POF and the other random copolymer $P(O_{50}/TE_{50}F)$. This result is in agreement with its random structure and the presence of only 20 mol % of TEF counits.

In the DSC curves of POF and of all the copolymers an additional small melting peak, located in the range 49–54 °C can be observed. Previous studies evidenced that its origin is different from crystal melting but can be ascribed to the formation of a mono- or bidimensional order, generally called mesophase. The presence in the macromolecular chain of mesogenic rings, like furan one, together with aliphatic moieties (octylene and triethylene) can give rise to this peculiar structure, [33,35,37,38] whose evidence can be seen in DSC trace as a small endothermic peak at temperature just above room temperature

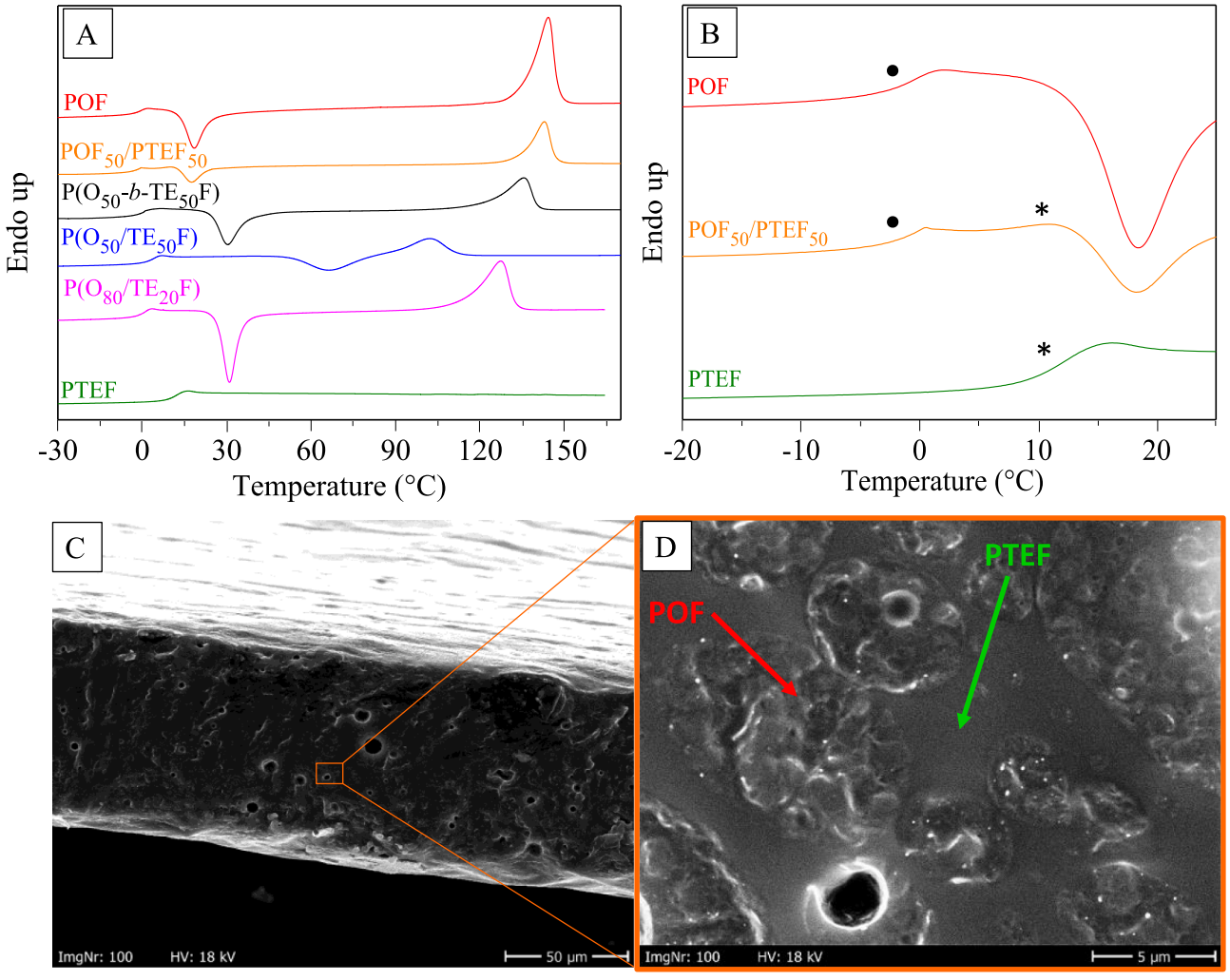

Fig. 4. A) II scan DSC curves of samples cooled from the molten state by immersion in liquid nitrogen and B) enlargement in the temperature range −20 °C - 25 °C of POF, PTEF and POF50/PTEF50 curves; C) SEM micrographs of $POF_{50}/PTEF_{50}$ film section at 500X and D) 5000X.

and well below T_m, associated to mesophase isotropization phenomenon. Interestingly, this peak position is independent on the composition and, surprisingly, increases in intensity when the crystallizing component (OF) decreases in amount ($P(O_{80}/TE_{20}F)$ vs $P(O_{50}/TE_{50}F)$) or in block length ($P(O_{50}$-*b*-$TE_{50}F)$ vs $P(O_{50}/TE_{50}F)$) [39].

The WAXD patterns of the tested samples are presented in Fig. 3C. As far as concerns homopolymer moieties, PTEF shows a bell-shaped profile typical of a fully amorphous material while POF is characterized by three stark peaks at angles of 24.0, 16.6 and 12.8°, in the order of decreasing intensity, with the addition of a 'bumped' baseline due to non-ordered component. The other samples display 'POF-type' pattern with peaks due to the same crystal phase, but with different content of the amorphous fraction as evident from the crystallinity degree values (X_c) reported in Table 2. The crystallinity degree values seem to be dependent on the OF counit amount, as a matter of fact X_c decreases with the OF content (POF > $P(O_{80}/TE_{20}F)$ > $P(O_{50}/TE_{50}F)$), but it is quite independent on the OF block length. As a matter of fact, all the polymers containing 50 mol % OF present X_c values of about 18 % regardless the OF block length. What is changing is the size of crystalline domains (L) estimated from the width of peak at 24° L decreases with the OF block length: it is 14 nm in POF homopolymer and blend, and reaches the minimum value of 9 nm in $P(O_{50}/TE_{50}F)$ random copolymer (Table 2).

As reported in the literature, [40,41] amorphous domains in a semicrystalline material generally have a different behaviour than in a completely amorphous material. Indeed, crystallinity acts as physical constraints, causing an increase in T_g value. For this reason, to study the dependence of the glass transition on the composition and architecture, it is better to observe the phenomenon in absence of crystallinity. Therefore, II DSC scans were performed after rapid cooling from the molten state, by immersing each sample in liquid nitrogen. The relative calorimetric curves and data are shown in Fig. 4A and listed in Table 2.

PTEF is the only sample which shows the same profile as I scan, with a T_g value of 11 °C, indicating the material is in the rubbery state at room temperature. Conversely, in all the other samples some remarkable differences can be observed with respect to I calorimetric scan. Indeed, once T_g is exceeded, an exothermic crystallization peak can be observed, indicating that macromolecular chains have enough energy to rearrange in an ordered crystalline structure, which melts at higher temperature.

Only for $P(O_{50}/TE_{50}F)$ quenching was effective, being $\Delta H_{cc} \approx \Delta H_m$. For POF, $P(O_{50}$-*b*-$TE_{50}F)$ and $P(O_{80}/TE_{20}F)$ copolymers and $POF_{50}/PTEF_{50}$ blend, only a portion of macromolecular chains was effectively quenched in the amorphous phase, but the effect was remarkable enough to allow the determination of T_g values.

As it can be seen from Table 2, all the materials are in the rubbery state at room temperature. More in detail, POF has a T_g value of −2 °C, while the values measured for the copolymers are located in between those of the two parent homopolymers and coherent with their chemical composition and architecture. This procedure was also useful to evidence the presence of two glass transition steps in the $POF_{50}/PTEF_{50}$ blend (Fig. 4B), located at −2 and 7 °C and associated to those of the two parent homopolymers (the lower to POF and the higher to PTEF, respectively). Looking more in depth, the T_g step at higher temperature is partially covered by the crystallization of OF segments, and this is probably the reason why its value is lower than the PTEF one. Of particular interest is the fact that crystallization of OF moieties starts only when the T_g of TEF moieties is exceeded, and at higher temperature with respect to POF homopolymer (Fig. 4B), meaning that PTEF in the glassy state hinders crystallization of POF. This evidence can be explained considering that although not chemically bounded and not miscible in the amorphous phase, POF and PTEF are intimately mixed. That suggests they could be at least compatible.

3.3. Blend morphology

To get a better insight on the morphology of $POF_{50}/PTEF_{50}$ blend, in Fig. 4C the SEM micrographs of blend film cross-sections at different enlargements are shown. From these micrographs interesting information on the blend morphology and the extent of the phase separation can be obtained.

From Fig. 4C one can see a smooth and continuous fracture surface indicating POF and PTEF components are well dispersed each other. Although the immiscibility of the two polymers was confirmed by DSC measurements, it seems that anyway their compatibility is good with small semicrystalline POF droplets (a few microns large) immersed in a continuous PTEF matrix, as evidenced in Fig. 4D Indeed, in a compatible polymeric blend, the two parent homopolymers are present in separate phases but the blend exhibits macroscopically uniform properties due to the strong interaction between the components of the blend.

3.4. Surface wettability

Surface wettability was performed by means of static contact angle measurements, carried out at different timepoints after deposition. In Fig. 5 drops pictures poured on polymeric surfaces at different timepoints after deposition are shown, together with the relative WCA values. As it can be seen, POF homopolymer is highly hydrophobic, as well as $POF_{50}/PTEF_{50}$ blend and $P(O_{80}/TE_{20}F)$ copolymer. In all cases, WCA was about 98–99 ° and the drop shape did not change after deposition. These results are in line with those obtained for other furan-based materials [36,42] Conversely, PTEF turned out to be the material with the highest hydrophilicity, with WCA value of 39° (Fig. 5), due to the presence of the ether oxygen atoms along the main chain, which confer PEG-like properties.

In case of the block and random copolymers containing 50 mol % TEF counit, although immediately after deposition WCA values are high (98° for $P(OF_{50}/TE_{50}F)$ and 85° for $P(O_{50}$-*b*-$TE_{50}F)$), an evolution of drop shape was recorded, WCA values getting lower after 30 s from deposition and, in case of $P(O_{50}$-*b*-$TE_{50}F)$, reaching a value of 73° after 1 min from deposition (Fig. 5). In this last case, a swelling of the surface in contact with water was also observed. The reason of this behavior can be explained with the presence of a consistent amount of TEF counits, which improve material hydrophilicity. Moreover, as already evidenced in previous studies, [43] although material hydrophilicity is expected to be the same (given the same chemical composition), a different behaviour was observed depending on the different molecular architecture, i.e. different block length, longer blocks being responsible of enhanced wettability. A possible explanation can be found in a hypothetic spatial reorganization of macromolecular chains, which leads hydrophilic TEF counits to interface with water, moving to the surface, and OF counits, more hydrophobic, to move inside the bulk, avoiding the contact with water. This behaviour, already studied in the literature, [44,45] is possible only when hydrophilic counits have enough energy to rearrange at room temperature, meaning that their T_g has to be below RT, as in the case of the polymers investigated. In addition, the minor decrease over time of WCA values of $P(OF_{50}/TE_{50}F)$ with respect to $P(O_{50}$-*b*-$TE_{50}F)$ can be explained considering the shorter OF as well as TEF blocks in the random copolymer (Table 2) and, as a consequence, the difficulty of generating quite large OF-rich and TEF-rich domains, characterized by different water affinity [43]

3.5. Mechanical characterization

To provide a deep insight into the mechanical properties of the materials under investigation, stress-strain measurements were carried out on polymeric films. The tensile testing data (elastic modulus E, stress at break σ_B and strain at break ε_B), are collected in Table 3, while stress-strain curves are shown in Fig. 6.

As known, mechanical properties are strictly related to molecular weight, the amount of crystalline phase, and chain mobility.

Both the homopolymers have the T_g below room temperature, which renders the polymer chain very mobile. POF homopolymer has a crystallinity degree of 37 %, which is responsible for the stiffness of the

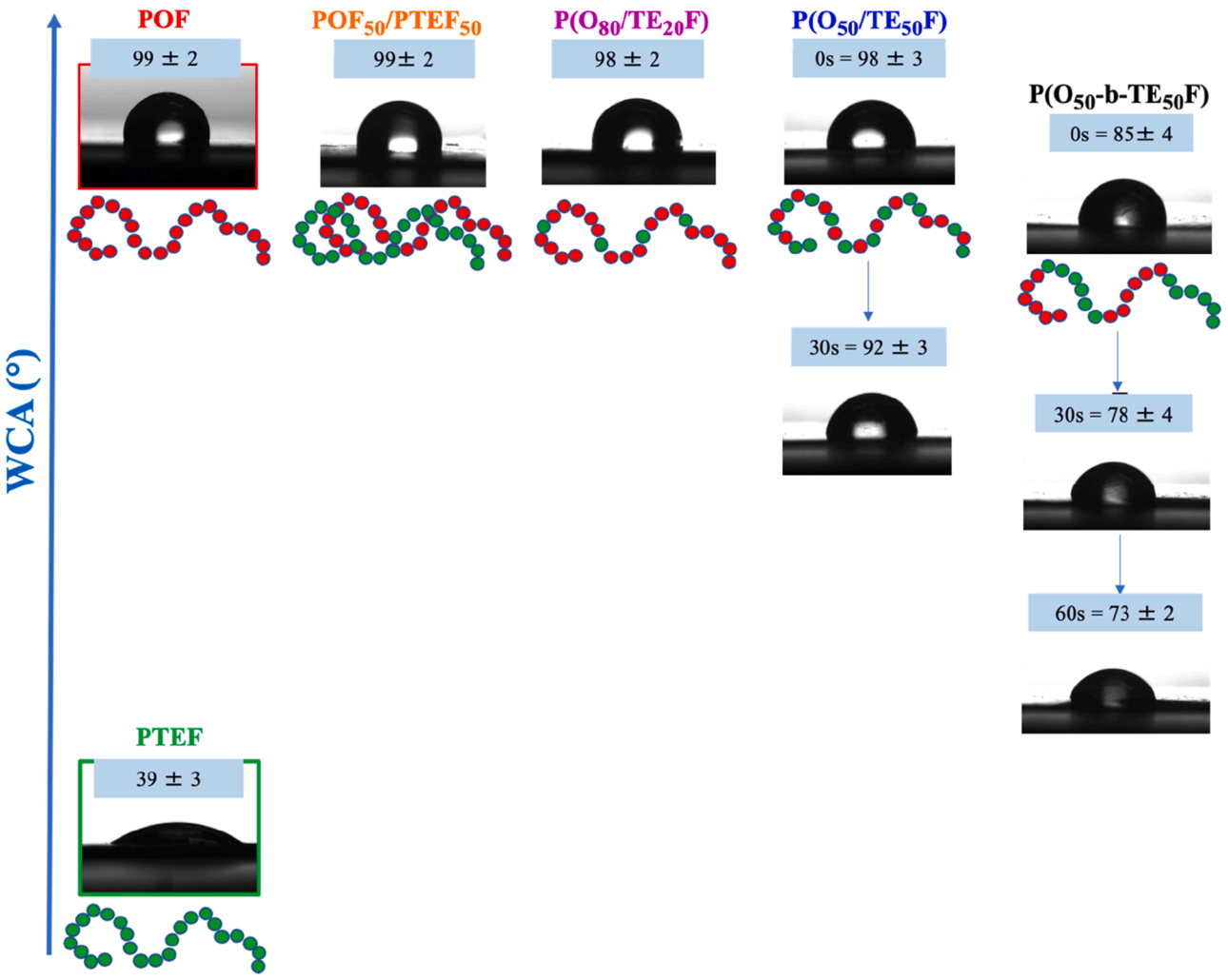

Fig. 5. WCA values and pictures of the water drop at different times after deposition for the materials under study.

Table 3
Mechanical and gas barrier data to O_2 and CO_2 (0 % RH and 85 % RH) of the materials under investigation.

	E (MPa)	σ_B (MPa)	ε_B (%)	O_2-TR 0 % RH cm^3cm/m^2 d atm	CO_2-TR 0 % RH cm^3cm/m^2 d atm	O_2-TR 85 % RH cm^3cm/m^2 d atm	CO_2-TR 85 % RH cm^3cm/m^2 d atm
POF	490 ± 70	26 ± 3	22 ± 2	1.02 ± 0.06	2.68 ± 0.08	0.20 ± 0.01	1.23 ± 0.05
POF_{50}/$PTEF_{50}$	26 ± 5	1.5 ± 0.2	184 ± 25	0.001 ± $5E^{-4}$	0.005 ± $5E^{-4}$	0.007 ± $5E^{-4}$	0.003 ± $5E^{-4}$
P(O_{50}-*b*-TE_{50}F)	88 ± 11	7 ± 1	51 ± 7	0.15 ± 0.02	1.24 ± 0.05	0.16 ± 0.02	1.16 ± 0.04
P(O_{50}/TE_{50}F)	89 ± 13	11 ± 2	553 ± 41	0.11 ± 0.01	1.12 ± 0.04	0.40 ± 0.02	1.05 ± 0.04
P(O_{80}/TE_{20}F)	290 ± 90	23 ± 4	308 ± 30	1.21 ± 0.06	2.35 ± 0.08	1.08 ± 0.04	2.22 ± 0.07
PTEF	-	-	1150 ± 50	-	-	-	-

material, while PTEF is completely amorphous. POF film is characterized by the highest elastic modulus (490 MPa) and stress at break (26 MPa) and the lowest elongation at break (22 %). Conversely, PTEF homopolymer is the one with the highest elongation at break, reaching values above 1100 %. Unfortunately, stress value remains particularly low during the entire test, which is the reason why it was not possible to determine *E* value. Anyway, by observing the inset in Fig. 6, it is possible to notice how the initial curve slope is the lowest among all the polymers tested. In the copolymers, the introduction of flexible PEG-like counits in POF backbone leads to significant differences in the mechanical response: a general decrease of elastic modulus and a higher elongation at break were observed, with variations depending on both the chemical composition (amount of TEF counits) and the chemical architecture (block or random). Reasonably, P(O_{80}/TE_{20}F), the copolymer containing the higher amount of OF counits presents the highest elastic modulus and stress at break, due to its high crystallinity, but still the elongation at break was remarkably increased, reaching a value of about 300 %. By increasing the TEF counits content to 50 mol %, in the P(O_{50}-*b*-TE_{50}F) and P(O_{50}/TE_{50}F) copolymers, elastic modulus about 5 times lower and stress at break values 3/4 times lower than that of POF, were achieved,

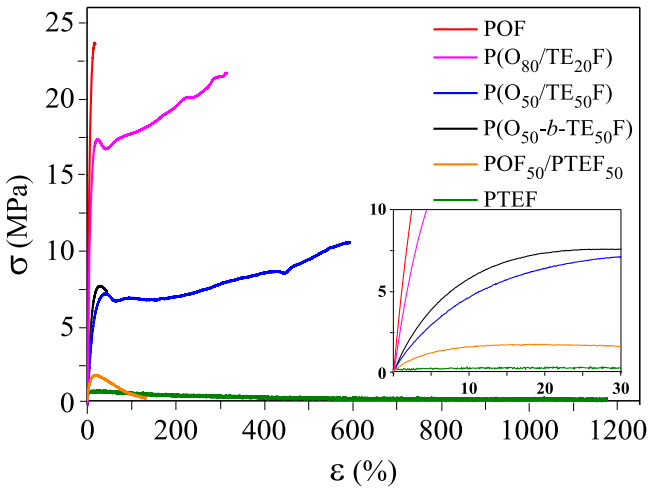

Fig. 6. Stress-strain curves of the materials under investigation. In the inset, the region corresponding to low stress and strain values is reported.

thanks to the flexibilization imparted by TEF segments. The effect of molecular architecture can be observed by comparing their elongation at break: 51 and 553 % for block and random copolymers, respectively. The significant difference cannot be ascribed to the crystallinity degree being X_c and ΔH_m values for the two copolymers comparable (Table 2) as well as their T_gs, i.e. same chain mobility. Anyway, as indicated by WAXS measurements, the block copolymer presents larger crystals with respect to the random one (Table 2). The lower elongation at break for P(O_{50}-*b*-TE_{50}F) could be also due to the slightly lower molecular weight (Table 1).

As to POF_{50}/$PTEF_{50}$ blend, the elastic modulus is more than ten times lower than the one of POF, with an elongation at break of almost 200 %, which is particularly remarkable considering that the homopolymers in the blend are not chemically bounded and the two phases are not miscible, according to DSC and SEM results (Fig. 4A and 4C). A similar evidence was already observed in the literature, but only with limited fraction of the second homopolymer (5–10 wt %) [44–46] Again, a possible explanation can be found in the presence of very small POF and PTEF domains, intimately mixed, characterized by a good dispersion and interfacial adhesion which confer to the blend very good mechanical properties.

Lastly, for all the copolymers and the blend, yielding can be observed after short elongations, in all cases below 40 %.

3.6. Gas barrier properties evaluation

The permeability tests to oxygen and carbon dioxide were carried out at 23 °C on the compression molded films of all the materials under study, in both dry (0 % RH) and humid (85 % RH) conditions. The permeability values, expressed as Gas Transmission Rate (GTR), are listed in Table 3 and shown in Fig. 7, together with those of some commercial plastics [47–49]. and other furan-based polymers, some of them previously investigated by the Authors [35,50,51]

As known, barrier properties are generally negatively influenced by all factors that increase free volume among chains, such as low T_g values and a high crystals/amorphous phase ratio. Indeed, lower T_g values mean higher amount of free volume leading to the increase of the gas transmission rate (GTR). Conversely, the presence of a substantial crystalline phase effectively hampers gas passage. As already mentioned, in furan-based polyesters the establishment of Van der Waals forces, π-π and polar interactions, [52–57] possibly producing mesophases, leads to outstanding barrier performance.

From the first test conducted at 23 °C in dry atmosphere, in case of PTEF a rapid gas passage through the polymeric matrix was observed. Despite the presence of ether-oxygen atom in PTEF repeating unit, which should enhance the number of hydrogen bonds (i.e. higher intermolecular forces), its T_g below room temperature and its complete amorphous nature play a predominant role favouring gas passage. Conversely, POF and P(O_{80}/TE_{20}F) copolymer show comparable values of GTR, considering the similar values of glass transition temperature and their high crystallinity degree. The introduction of consistent amounts of TEF moieties (50 mol %), regardless of the molecular architecture, did not negatively affect the barrier performance of the copolymers but rather is responsible of an improvement of about 10 times for O_2 and of 2 times for CO_2. As known from previous studies, [33,35,42] the formation of crystalline phase and the consequent increase in interphase regions (between crystalline and amorphous domains) in furan-based materials can reduce their very good gas barrier ability. In this view, the lower crystallinity degree in the copolymers with respect to POF can be an advantage in terms of gas barrier. A quite surprising and uncommon result was obtained for POF_{50}/$PTEF_{50}$ blend, whose GTR values to O_2 and CO_2 were 0.001 and 0.005 cm^3cm/m d atm, respectively, about 3 and 2.5 orders of magnitude lower than POF. Again, this result can be explained by the outstanding compatibility between POF and PTEF homopolymers, with small POF domains intimately mixed to PTEF regions (as confirmed by SEM analysis), to form a microscopically dense structure particularly effective in hampering gas passage. Another point to take into account is the rubbery amorphous

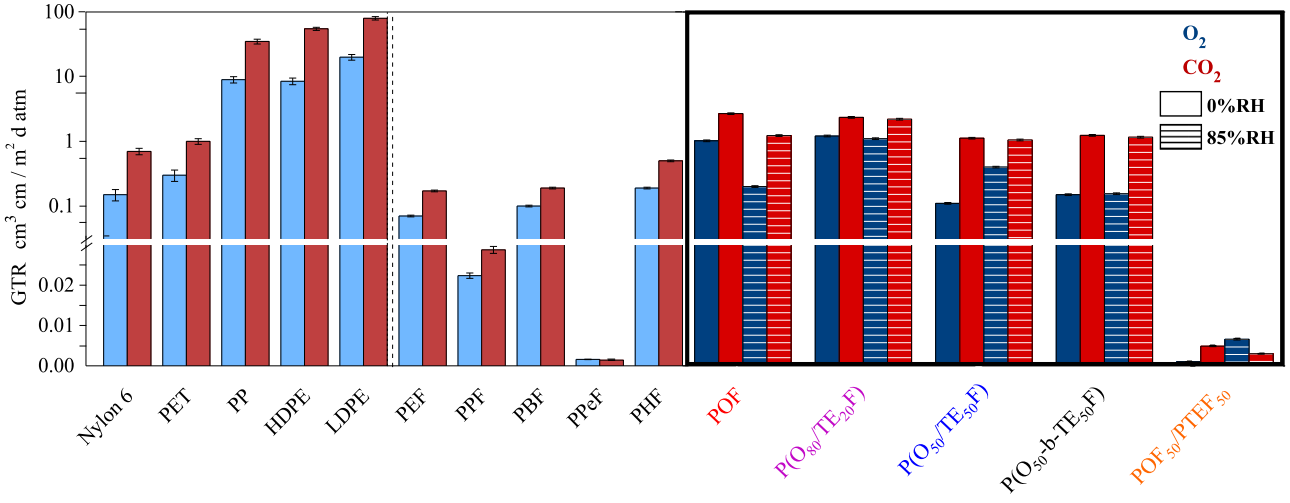

Fig. 7. GTR values of the materials under investigation in dry (0 % RH) and wet (85 % RH) conditions. Comparison with some commercial plastics [47–49] and other furan-based homopolymers [35,50,51].

nature of PTEF homopolymer that allow it to perfectly fill out the voids in the semicrystalline POF matrix. Similar results have been previously reported in the literature for physical blends containing rubbery amorphous furan-based component [58]

Afterwards, the films were subjected to permeability tests at 85 % RH, keeping the temperature constant at 23 °C. In case of POF and all the copolymers, permeability values remained almost unaltered, making these materials very performant also in humid environments.

In the case of the blend, an increase of GTR values to oxygen was observed. The result is not surprising considering the plasticizing effect of water, which enhances chain mobility, thus causing an increment of free volume [59,60]

If the permeabilities to the two gases are compared, in all cases CO_2-TR is higher than O_2-TR, meaning carbon dioxide passed through the films easier than O_2, in line with previous studies [61,62] Oxygen is a small (molecular diameter of 3.1 Å) no-polar molecule, while carbon dioxide is bigger (molecular diameter of 3.4 Å) [63] and contains polar C—O covalent bonds. These different characteristics make oxygen its transmission rate is usually lower than carbon dioxide.

A peculiar behaviour is represented by the blend in humid environment, in which CO_2-TR turns lower than O_2-TR. To explain this result, one has to consider several factors: water molecules can exert a plasticizing effect, i.e. rise free volume, but can also increase the interchain interactions by forming water-bridges and ultimately affect gas solubility in the polymer matrix.

In Fig. 7, a comparison of GTR values to dry gases has been made with respect to PET, which dominates the market of beverage packaging, and other commodities [47–49]. In all cases the materials under study are characterized by comparable or even better performance, making them vary attracting as sustainable alternatives. If compared to other furan-based polyesters, [35,50,51] the samples under study are characterized by performances similar to poly(hexamethylene 2,5-furanoate) (PHF).

The only exception is represented by the blend, whose outstanding gas barrier behavior is comparable to poly(pentamehtylene 2,5-furanoate) (PPeF), the most outstanding furan-based material [42] This evidences just the physical blending of POF and PTEF is particularly effective in enhancing the gas-barrier properties of both the homopolymers, which opens the way for the application of POF/PTEF blends in the food packaging field.

3.7. Compostability evaluation

Compostability is a feature of particular importance in case of packages with short life-cycle and contaminated by food. Indeed, compostable materials can avoid the accumulation of wastes in landfill, in particular where recycling is not a feasible option.

To check their biodegradability, all the materials investigated have been subjected to lab-scale composting experiments. Percentage gravimetric weight loss as a function of composting time is reported in Fig. 8A. This value is practically negligible for POF and P(O_{80}/TE_{20}F) even at longer incubation times (180 days). On the contrary, PTEF homopolymer completely degraded within 24 h. From Fig. 8B it is possible also to see how degradation starts immediately after incubation, and after only one hour only small pieces of film are present. POF_{50}/$PTEF_{50}$, P(O_{50}-*b*-TE_{50}F) and P(O_{50}/TE_{50}F) underwent degradation with a rate which is intermediate between those of their two parent homopolymers. More in detail, the blend degraded within 14 days, the block one in 45 days, while for the random copolymer degradation occurred in 14 days. This evidence can be explained, in the copolymers, by considering the lower degree of crystallinity as well as the higher hydrophilicity, with respect to POF (Fig. 5 and Table 2). For the blend, the result can be correlated only to the lower crystallinity (Table 2), being the WCA value comparable to the one of POF (Fig. 5). As well known, both these parameters favor microbial attack. In particular, in the case of POF_{50}/$PTEF_{50}$ the fact that the two homopolymers are only physically blended

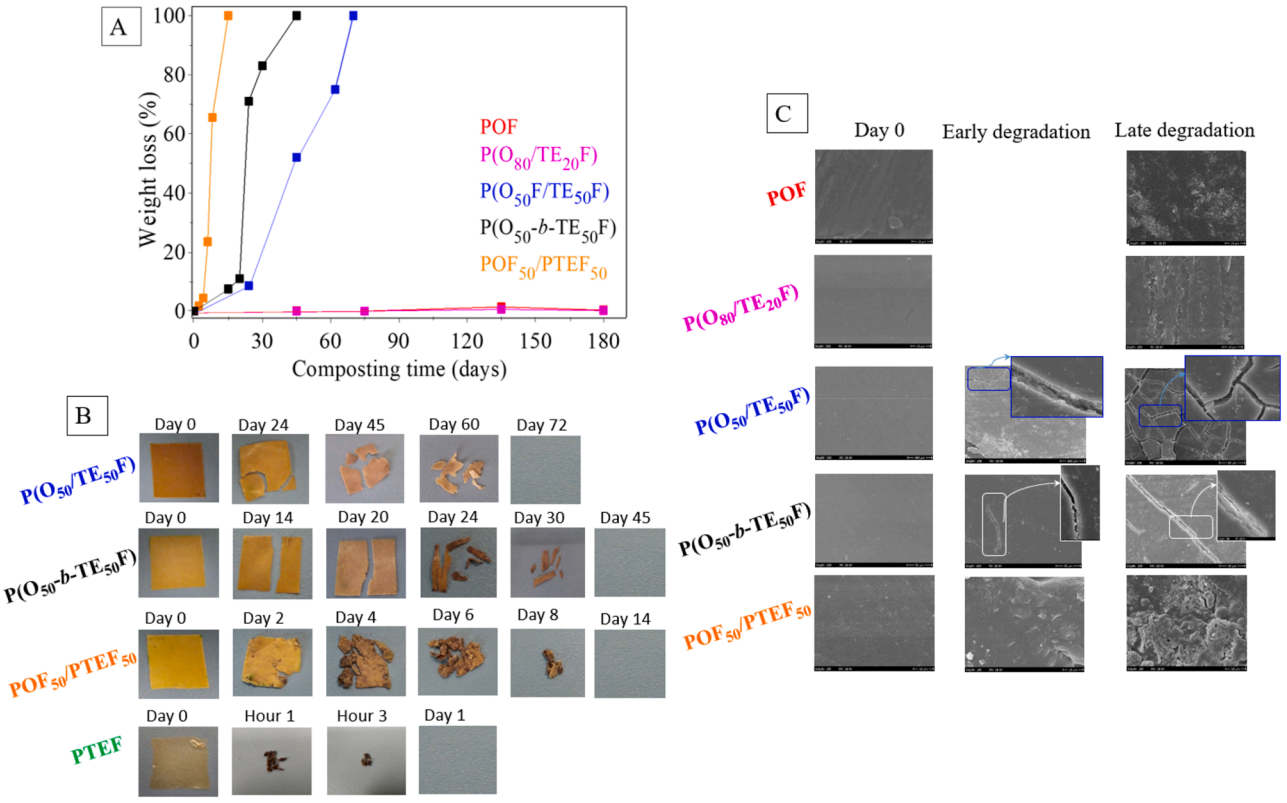

Fig. 8. A) Percentage gravimetric weight loss as a function of composting time; B) Evolution of samples' shape and color after composting experiments at different timepoints and C) SEM pictures of the materials investigated before degradation, at shorter degradation times and longer degradation times.

can explain how the degradation rate was so high: it is possible that the degradation of PTEF chains, which were not chemically linked to POF ones, created holes in the film, through which enzymes could pass and start degradation of the remaining POF Macromolecules As to the copolymers, the weight loss was faster for the copolymer containing longer blocks compared to the one containing shorter ones. In the literature, different trends have been reported for block copolymers degradation rate [27,43] In general, the shorter the block the faster the degradation, as a consequence of lower crystallinity degree of shorter block copolymers. In the present study, one has to consider that all the copolymers have similar melting enthalpy regardless the block length. On the other hand, the results evidenced higher hydrophilicity of P(O_{50}-*b*-TE_{50}F) with respect to P(O_{50}/TE_{50}F), in particular at longer times (Table 1). Therefore, it is possible water and enzymes more easily attack longer hydrophilic TEF blocks, since shorter ones are less accessible due to the proximity to hydrophobic POF blocks. Indeed, composting experiments were carried out in wet compost (RH > 95 %).

Anyway, all these results confirm the effectiveness of the modification of POF, by introducing PEG-like segments, in terms of compost degradation rate, making these materials suitable for the realization of compostable single-use packaging. A deep analysis of partially degraded samples by means of ^{1H}NMR^{1}H-NMR and DSC was carried out on P(O_{50}-*b*-TE_{50}F) block copolymer, in order to check any variation in chemical composition and thermal transitions. Composition variation was monitored observing ^{1}H-NMR of partially degraded samples, focusing on the peaks of *f* methylene protons of triethylene subunit and peaks of *b* protons of octylene one. As evidenced by Fig. 1B, and reported in Table 4, the TEF counits content gradually decreases in the partially degraded samples, starting from 49 mol % and reaching values of 42, 41, 36 and 34 mol % after 14, 20, 24 and 30 days, respectively. The reduction of the triethylene furanoate segments is also responsible for the increase in the crystallinity degree of the material, as confirmed by DSC analysis. In fact, as shown in Table 4 and in Figure 3D, where a magnification in the temperature range 90–170 °C is shown, the melting peak located at 136 °C becomes higher and more pronounced, by increasing the incubation time, with a parallel increase of ΔH_m values.

The degradation process has been also evaluated through a macroscopic analysis of the surface. In Fig. 8B, pictures of partially degraded PTEF, POF_{50}/$PTEF_{50}$, P(O_{50}-*b*-TE_{50}F) and P(O_{50}/TE_{50}F) at different timepoints, compared to the same samples before degradation experiments, are reported (for POF and P(O_{80}/TE_{20}F) no remarkable changes were observed). After only one hour, PTEF was completely permeated by compost and only small pieces were withdrawn from incubation. All the other films became progressively darker and more fragile with incubation time, with a consistent fragmentation at longer times.

Scanning electron microscopy (SEM) pictures of the materials were collected before degradation, at shorter and longer degradation times. All the pictures are shown in Fig. 8C. As it can be seen, despite the almost negligible weight loss, the surfaces of POF and P(O_{80}/TE_{20}F) films after 6 months of incubation show different points of attack by microorganisms, indicating that, even at slower rate the degradation process affects these polymers too. In the case of POF_{50}/$PTEF_{50}$, P(O_{50}-*b*-TE_{50}F) and P(O_{50}/TE_{50}F), as already suggested by the weight loss results, a considerable deterioration of material was observed also at the micrometric level because of the microbial attack extended to the whole surface. In particular, the formation of cracks in the case of the copolymers and holes in the case of the blend was detected, suggesting two different degradation mechanisms: predominantly hydrolytic in the first case, predominantly enzymatic in the second one [64,65]. The results evidenced the impact of chemical vs physical blending on the degradation mechanism: when the two homopolymer are chemically connected, bulky hydrolysis prevails leading to cracks formation; when POF and PTEF are just physically blended, surface erosion also occurs. No effect of block length nor hydrophilicity can be evidenced.

Table 4
^{1H1}NMRH-NMR and DSC characterization data of partially degraded samples as a function of incubation time in compost.

Incubation time (Days)	TEF (mol%)	T_m°C	ΔH_m J/g
0	49	136	21.3
14	42	137	25.9
20	41	137	27.5
24	36	137	28.2
30	34	137	29.9

4. Conclusions

The present work is a case of study of chemical design for achieving the desired functional properties according to the envisioned application.

The reference furan-based homopolymer poly(octylene 2,5-furanoate) (POF) has been modified by combining it with another homopolyester of FDCA, poly(triehtylene 2,5-furanoate) (PTEF), with very similar chemical structure to promote good compatibility between the two matrices. As a matter of fact, POF and PTEF differ just for the presence of two ether oxygen atoms instead of two -CH_2- groups in the glycol subunits of PTEF with respect to POF, but resulting in very different solid-state properties. Indeed, POF is a semicrystalline and hydrophobic material with good gas barrier performance but a very stiff and brittle mechanical behavior, while the presence of ether oxygen atoms in PTEF is responsible for high hydrophilicity and mechanical flexibility. Against, its rubbery amorphous state at room temperature makes PTEF not effective in blocking gas molecules passage.

Proper chemical design allowed a fine tuning of the solid-state properties by acting on:

- Physical/chemical blending
- Counit amount, keeping fixed the molecular architecture (random distribution)
- Block length, keeping fixed the composition (equimolar)

In all the obtained materials the high thermal stability, typical of furan-based polyesters, was kept, as well as quite high crystallinity degree, this last of fundamental importance in terms of material processing and dimensional stability. Calorimetric measurements also show the formation of mesophase in the copolymers with lower OF segment length. This kind of arrangement could contribute to the maintenance or even improvement of O_2 and CO_2 barrier ability with respect to POF homopolymer. Both wettability and mechanical properties were tuned as a result of chemical structure and composition as well as molecular architecture: hydrophilic character, flexibility and toughness enhanced by reducing block length. Melting temperature progressively reduced when block length decreased, as a consequence of crystal size reduction, while melting enthalpy keeps constant. Lastly, the composting experiments confirmed the possibility to progressively speed up degradation process by decreasing block length.

Particularly surprising was the equimolar physical blend. First, this was the easiest material to realize, using the mildest conditions, without the need of reducing the pressure or increasing temperature and time, which are all features that make the material easy to scale up even at industrial level. Moreover, it presents very performing mechanical properties, with a quite high resistance and remarkable elongation at break. This evidence is of a particular interest, taking into account that POF and PTEF are just physically mixed together. Last, this material turned out to be compostable in only two weeks and the most performing in terms of gas barrier properties. Such an outstanding behaviour has been explained as due to the high compatibility between POF and PTEF homopolymers, reached without using any compatibilizer, with small POF domains intimately mixed to PTEF regions to form a microscopically dense structure particularly effective in hampering gas passage. This hypothesis was supported by SEM analysis.

In conclusion, the choice of the proper parent homopolymers, together with the *ad hoc* chemical design were very effective in obtaining materials suitable for sustainable flexible food packaging that are recyclable or compostable.

Synopsis

Novel furan-based polyesters with different composition and molecular architecture are prepared for the realization of sustainable, flexible and recyclable/compostable food packaging.

CRediT authorship contribution statement

Giulia Guidotti: Writing – original draft, Methodology, Investigation, Formal analysis, Data curation. **Michelina Soccio:** Writing – original draft, Validation, Supervision, Resources, Project administration, Funding acquisition, Data curation, Conceptualization. **Valentina Siracusa:** Writing – review & editing, Validation, Supervision, Methodology, Investigation, Formal analysis, Data curation. **Elisabetta Salatelli:** Writing – review & editing, Validation, Methodology, Investigation, Formal analysis, Data curation. **Nadia Lotti:** Writing – review & editing, Supervision, Resources, Project administration, Funding acquisition, Conceptualization.

Declaration of competing interest

The authors declare that they have no known competing financial interests or personal relationships that could have appeared to influence the work reported in this paper.

Acknowledgments

G.G., M.S., N.L., acknowledge the Italian Ministry of University and Research.

This research was funded by the Agritech National Research Center and received funding from the European Union Next-GenerationEU (PIANO NAZIONALE DI RIPRESA E RESILIENZA (PNRR)—MISSIONE 4 COMPONENTE 2, INVESTIMENTO1.4—D.D. 1032 17/06/2022, CN00000022). This manuscript reflects only the authors' views and opinions; neither the European Union nor the European Commission can be considered responsible for them.

Data availability

Data will be made available on request.

References

[1] R. Kumar, A. Verma, A. Shome, R. Sinha, S. Sinha, P.K. Jha, R. Kumar, P. Kumar, Shubham, S. Das, P. Sharma, P.V. Vara Prasad, Impacts of plastic pollution on ecosystem services, sustainable development goals, and need to focus on circular economy and policy interventions, Sustainability 13 (2021) 9963, https://doi.org/10.3390/su13179963.

[2] S.B. Obebe, A.A. Adamu, Adamu. Plastic pollution: causes, effects and preventions, IJEAST 4 (2020) 85–95.

[3] A.M. Yatoo, B. Hamid, T.A. Sheikh, S. Ali, S.A. Bhat, S. Ramola, M.N. Ali, Z. A. Baba, S. Kumar, Global perspective of municipal solid waste and landfill leachate: generation, composition, eco-toxicity, and sustainable management strategies, Environ. Sci. Pollut. Res. 31 (2024) 23363–23392, https://doi.org/10.1007/s11356-024-32669-4.

[4] D. Knoblauch, L. Mederake, Government policies combatting plastic pollution, Curr. Opin. Toxicol. 28 (2021) 87–96, https://doi.org/10.1016/j.cotox.2021.10.003.

[5] A. Hira, H. Pacini, K. Attafuah-Wadee, D. Vivas-Eugui, M. Saltzberg, T.N. Yeoh, Plastic waste mitigation strategies: a review of lessons from developing countries, J. Dev. Soc. 38 (3) (2022) 336–359, https://doi.org/10.1177/0169796X221104855.

[6] United Nations Environment Programme, Policy options to eliminate additional marine plastic litter 2021, https://wedocs.unep.org/bitstream/handle/20.500.11822/36440/POEAMPL.pdf.

[7] G20 (2017). G20 Action plan on marine litter 2017. https://www.mofa.go.jp/mofaj/files/000272290.pdf.

[8] P. Ghisellini, C. Cialani, S. Ulgiati, A review on circular economy: the expected transition to a balanced interplay of environmental and economic systems, J. Clean. Prod. 114 (2016) 11–32, https://doi.org/10.1016/j.jclepro.2015.09.007.

[9] Decision No 1386/2013/EU of the European parliament and of the Council of 20 November 2013 on a general union environment action programme to 2020 'living well, within the limits of our planet'. https://www.legislation.gov.uk/eudn/2013/1386/2020-01-31.

[10] Plastics Europe, Plastics, the facts 2022. https://plasticseurope.org/knowledge-hub/plastics-the-facts-2022/.

[11] I.A. Idowu, W. Atherton, K. Hashim, P. Kot, R. Alkhaddar, B.I.Alo Alo, A. Shaw, An analyses of the status of landfill classification systems in developing countries: sub Saharan Africa landfill experiences, Waste Manage. 87 (2019) 761–771, https://doi.org/10.1016/j.wasman.2019.03.011.

[12] N. Ferronato, V. Torretta, Waste mismanagement in developing countries: a review of global issues, Int. J. Environ. Res. Public Health 16 (6) (2019) 1060, https://doi.org/10.3390/ijerph16061060.

[13] R. Geyer, J.R. Jambeck, K.L. Law, Production, use, and fate of all plastics ever made, Sci. Adv. 3 (7) (2017) e1700782, https://doi.org/10.1126/sciadv.1700782.

[14] Plastic Market Size, Share & trends analysis report by product (PE, PP, PU, PVC, PET, Polystyrene, ABS, PBT, PPO, Epoxy Polymers, LCP, PC, Polyamide), by application, by end-use, by region, and segment forecasts, 2023–2030. https://www.researchandmarkets.com/reports/4751797/plastic-market-size-share-and-trends-analysis?srsltid=AfmBOopB-bys3RxL25fEUqzG5P03c5HA_Mfoqwr-SH5OfkjN9Pp7gCac.

[15] Plastics, the fast facts, 2024. https://plasticseurope.org/knowledge-hub/plastics-the-fast-facts-2024/.

[16] https://www.flexpack-europe.org.

[17] F. Wu, M. Misra, A.K. Mohanty, Challenges and new opportunities on barrier performance of biodegradable polymers for sustainable packaging, Prog. Polym. Sci. 117 (2021) 101395, https://doi.org/10.1016/j.progpolymsci.2021.101395.

[18] Y. Ciawi, S.G. Tonyes, N.M. Utami Dwipayanti, Multilayer packaging recycling: challenges, current practices, and future prospects, Acad. Env. Sci. Sust. 2 (2025) 1–12, https://doi.org/10.20935/AcadEnvSci7521.

[19] Q. Zhang, M. Song, Y. Xu, W. Wang, Z. Wang, L. Zhang, Bio-based polyesters: recent progress and future prospects, Prog. Polym. Sci. 120 (2021) 101430, https://doi.org/10.1016/j.progpolymsci.2021.101430.

[20] A. Gandini, T.M. Lacerda, Furan polymers: state of the art and perspectives, Macromol. Mater. Eng. 307 (2022) 2100902, https://doi.org/10.1002/mame.202100902.

[21] K. Loos, R. Zhang, I. Pereira, B. Agostinho, H. Hu, D. Maniar, N. Sbirrazzuoli, A.J. D. Silvestre, N. Guigo, A.F. Sousa, A perspective on PEF synthesis, properties, and end-life, Front. Chem. 8 (2020) 585, https://doi.org/10.3389/fchem.2020.00585.

[22] Z. Terzopoulou, L. Papadopoulos, A. Zamboulis, D.G. Papageorgiou, G. Z. Papageorgiou, D.N. Bikiaris, Tuning the properties of furandicarboxylic acid-based polyesters with copolymerization: a review, Polymers 12 (2020) 1209, https://doi.org/10.3390/polym12061209.

[23] H. Hu, R. Zhang, J. Wang, W. Bin Ying, L. Shi, C. Yao, Z. Kong, K. Wang, J. Zhu, A mild method to prepare high molecular weight poly(butylene furandicarboxylate-co-glycolate) copolyesters: effects of the glycolate content on thermal, mechanical, and barrier properties and biodegradability, Green. Chem. 21 (2019) 3013–3022, https://doi.org/10.1039/c9gc00668k.

[24] S. Peng, B.S. Wu, L. Wu, B.G. Li, P. Dubois, Hydrolytic degradation of biobased poly(butylene succinate-co-furandicarboxylate) and poly(butylene adipate-cofurandicarboxylate) copolyesters under mild conditions, J. Appl. Polym. Sci. 134 (2017) 44674, https://doi.org/10.1002/app.44674.

[25] A. Zubkiewicz, A. Szymczyk, R.J. Sablong, M. Soccio, G. Guidotti, V. Siracusa, N. Lotti, Bio-based aliphatic/aromatic poly(trimethylene furanoate/sebacate) random copolymers: correlation between mechanical, gas barrier performances and compostability and copolymer composition, Polym. Degrad. Stab. 195 (2022) 1–16, https://doi.org/10.1016/j.polymdegradstab.2021.109800.

[26] E. Bianchi, G. Guidotti, M. Soccio, V. Siracusa, M. Gazzano, E. Salatelli, N. Lotti, Biobased and compostable multiblock copolymer of poly(L-lactic acid) containing 2,5-furandicarboxylic acid for sustainable food packaging: the role of parent homopolymers in the composting kinetics and mechanism, Biomacromolecules 24 (2023) 2356–2368, https://doi.org/10.1021/acs.biomac.3c00216.

[27] A. Zubkiewicz, A. Szymczyk, J. Dryzek, Z. Rozwadowski, R.J. Sablong, M. Soccio, G. Guidotti, V. Siracusa, N. Lotti, Superior barrier performance, mechanical properties and compostability in relation to supramolecular structure of renewable based poly(trimethylene furanoate) modified with suberic acid, Eur. Polym. J. 223 (2025) 113673, https://doi.org/10.1016/j.eurpolymj.2024.113673.

[28] G.Z. Papageorgiou, N. Guigo, V. Tsanaktsis, D.G. Papageorgiou, S. Exarhopoulos, N.;. Sbirrazzuoli, D.N. Bikiaris, On the bio-based furanic polyesters: synthesis and thermal behavior study of poly(octylene furanoate) using fast and temperature modulated scanning calorimetry, Eur. Polym. J. 68 (2015) 115–127, https://doi.org/10.1016/j.eurpolymj.2015.04.011.

[29] Z. Terzopoulou, V. Tsanaktsis, M. Nerantzaki, D.S. Achilias, T. Vaimakis, G. Z. Papageorgiou, D.N. Bikiaris, Thermal degradation of biobased polyesters: kinetics and decomposition mechanism of polyesters from 2,5-furandicarboxylic acid and long-chain aliphatic diols, J. Anal. Appl. Pyrolysis. 117 (2016) 162–175, https://doi.org/10.1016/j.jaap.2015.11.016.

[30] M. Fabbri, G. Guidotti, M. Soccio, N. Lotti, M. Govoni, E. Giordano, M. Gazzano, R. Gamberini, B. Rimini, A. Munari, Novel biocompatible PBS-based random copolymers containing PEG-like sequences for biomedical applications: from drug

delivery to tissue engineering, Polym. Degrad. Stab. 153 (2018) 53–62, https://doi.org/10.1016/j.polymdegradstab.2018.04.011.
[31] N. Lotti, L. Finelli, M. Fiorini, M.C. Righetti, A. Munari, Synthesis and characterization of poly(butylene terephthalate-co-triethylene terephthalate) copolyesters, J. Appl. Polym. Sci. 81 (2001) 981–990, https://doi.org/10.1002/app.1520.
[32] M. Gigli, N. Lotti, M. Gazzano, V. Siracusa, L. Finelli, A. Munari, M. Dalla Rosa, Biodegradable aliphatic copolyesters containing PEG-like sequences for sustainable food packaging applications, Polym. Degrad. Stab. 105 (2014) 96–106, https://doi.org/10.1016/j.polymdegradstab.2014.04.006.
[33] S. Quattrosoldi, G. Guidotti, M. Soccio, V. Siracusa, N. Lotti, Bio-based and one-day compostable poly(diethylene 2,5-furanoate) for sustainable flexible food packaging: effect of ether-oxygen atom insertion on the final properties, Chemosphere 291 (2022) 132996, https://doi.org/10.1016/j.chemosphere.2021.132996.
[34] H.P. Klug, L.E. Alexander, X-Ray Diffraction Procedures, John Wiley & Sons Inc. 2nd Ed, 1974, pp. 687–703.
[35] G. Guidotti, M. Soccio, M.C. García-Gutiérrez, T.A. Ezquerra, V. Siracusa, E. Gutiérrez-Fernández, A. Munari, N. Lotti, Fully biobased superpolymers of 2,5-furandicarboxylic acid with different functional properties: from rigid to flexible, high performant packaging materials, ACS. Sustain. Chem. Eng. 8 (2020) 9558–9568, https://doi.org/10.1021/acssuschemeng.0c02840.
[36] G. Guidotti, M. Soccio, N. Lotti, V. Siracusa, M. Gazzano, A. Munari, New multi-block copolyester of 2,5-furandicarboxylic acid containing PEG-like sequences to form flexible and degradable films for sustainable packaging, Polym. Degrad. Stab. 169 (2019) 108963, https://doi.org/10.1016/j.polymdegradstab.2019.108963.
[37] G. Guidotti, M. Soccio, M. Gazzano, V. Siracusa, N. Lotti, Poly(Alkylene 2,5-Thiophenedicarboxylate) polyesters: a new class of bio-based high-performance polymers for sustainable packaging, Polymers 13 (2021) 2460, https://doi.org/10.3390/polym13152460.
[38] G. Guidotti, M. Gigli, M. Soccio, N. Lotti, M. Gazzano, V. Siracusa, A. Munari, Ordered structures of poly(butylene 2,5-thiophenedicarboxylate) and their impact on material functional properties, Eur. Polym. J. 106 (2018) 284–290, https://doi.org/10.1016/j.eurpolymj.2018.07.027.
[39] M. Soccio, M. Costa, N. Lotti, M. Gazzano, V. Siracusa, E. Salatelli, P. Manaresi, A. Munari, Novel fully biobased poly(butylene 2,5-furanoate/diglycolate) copolymers containing ether linkages: structure-property relationships, Eur. Polym. J. 81 (2016) 397–412, https://doi.org/10.1016/j.eurpolymj.2016.06.022.
[40] L.H. Sperling, Introduction to Physical Polymer Science, 6, Wiley, 2005, p. 8. Third edition, chapters 5.
[41] A.A. Askadskii, M. Popova, T. Matseevich, E. Kurskaya, The influence of the degree of crystallinity on the glass transition temperature of polymers, Adv. Mater. Res. 864-867 (2013) 751–754, https://doi.org/10.4028/www.scientific.net/AMR.864-867.751.
[42] G. Guidotti, M. Soccio, M.C. García-Gutierrez, E. Gutierrez-Fernandez, T. A. Ezquerra, V. Siracusa, A. Munari, N. Lotti, Evidence of a 2D-ordered structure in biobased poly(pentamethylene furanoate) responsible for its outstanding barrier and mechanical properties, ACS. Sustain. Chem. Eng. 7 (2019) 17863–17871, https://doi.org/10.1021/acssuschemeng.9b04407.
[43] C. Gualandi, M. Soccio, E. Saino, M.L. Focarete, N. Lotti, A. Munari, L. Moroni, L. Visai, Easily synthesized novel biodegradable copolyesters with adjustable properties for biomedical applications, Soft. Matter. 8 (2012) 5466, https://doi.org/10.1039/C2SM25308A.
[44] P. Theato, M. Brehmer, L. Conrad, C.W. Frank, L. Funk, D.Y. Yoon, J. Luning, Surface reorganization of an amphiphilic block copolymer film studied by NEXAFS spectroscopy, Macromolecules 39 (2006) 2592–2595, https://doi.org/10.1021/ma0509964.
[45] S.H. Anastasiadis, H. Retsos, S. Pispas, N. Hadjichristidis, S. Neophytides, Smart polymer surfaces, Macromolecules 36 (2003) 1994–1999, https://doi.org/10.1021/ma0211129.
[46] D. Rigotti, M. Soccio, A. Dorigato, M. Gazzano, V. Siracusa, G. Fredi, N. Lotti, Novel biobased polylactic acid/poly(pentamethylene 2,5-furanoate) blends for sustainable food packaging, ACS Sustainable Chem. Eng. 9 (2021) 13742–13750, https://doi.org/10.1021/acssuschemeng.1c04092.
[47] G. Fredi, D. Rigotti, D.N. Bikiaris, A. Dorigato, Tuning thermo-mechanical properties of poly(lactic acid) films through blending with bioderived poly (alkylene furanoate)s with different alkyl chain length for sustainable packaging, Polymers 218 (2021) 123527, https://doi.org/10.1016/j.polymer.2021.123527.
[48] Y. Long, R. Zhang, J. Huang, J. Wang, Y. Jiang, G.-h. Hu, J. Yang, J. Zhu, Tensile property balanced and gas barrier improved poly(lactic acid) by blending with biobased poly(butylene 2,5-furan dicarboxylate), ACS Sustainable Chem. Eng. 5 (2017) 9244–9253, https://doi.org/10.1021/acssuschemeng.7b02196.
[49] G. Mensitieri, E. Di Maio, G.G. Buonocore, I. Nedi, M. Oliviero, L. Sansone, S. Iannace, Processing and shelf life issues of selected food packaging materials and structures from renewable resources, Trends. Food Sci. Technol. 22 (2011) 72–80, https://doi.org/10.1016/j.tifs.2010.10.001.
[50] S.K. Burgess, R.M. Kriegel, W.J. Koros, Carbon dioxide sorption and transport in amorphous poly(ethylene furanoate), Macromolecules 48 (2015) 2184–2193, https://doi.org/10.1021/acs.macromol.5b00333.
[51] S.K. Burgess, O. Karvan, J.R. Johnson, R.M. Kriegel, W.J. Koros, Oxygen sorption and transport in amorphous poly(ethylene furanoate), Polymers 55 (2014) 4748–4756, https://doi.org/10.1016/j.polymer.2014.07.041.
[52] V.Y. Rudyak, A.A. Gavrilov, D.V. Guseva, S.H. Tung, P.V. Komarov, Accounting for π–π stacking interactions in the mesoscopic models of conjugated polymers, Mol. Syst. Des. Eng. 5 (2020) 1137–1146, https://doi.org/10.1039/D0ME00034E.
[53] A. Shanavas, S. Sathiyaraj, A. Chandramohan, T. Narasimhaswamy, Sultan Nasar, A. Isophthalic acid based mesogenic dimers: synthesis and structural effects on mesophase properties, J. Mol. Struct. 1038 (2013) 126–133, https://doi.org/10.1016/j.molstruc.2013.01.047.
[54] A. Mahendrasingam, D.J. Blundell, C. Martin, V. Urban, T. Narayanan, W. Fuller, Time resolved WAXS study of the role of mesophase in oriented crystallisation of poly(ethylene terephthalate-co-isophthalate) copolymers, Polymers 46 (2005) 6044–6049, https://doi.org/10.1016/j.polymer.2005.04.091.
[55] M.M. Nolasco, C.F. Araujo, S. Thiyagarajan, S. Rudić, P.D. Vaz, A.J.D. Silvestre, P. J.A. Ribeiro-Claro, A.F.Asymmetric Monomer Sousa, Amorphous polymer? Structure–Property relationships in 2,4-FDCA and 2,4-PEF, Macromolecules 53 (2020) 1380–1387, https://doi.org/10.1021/acs.macromol.9b02449.
[56] S.K. Burgess, J.E. Leisen, B.E. Kraftschik, C.R. Mubarak, R.M. Kriegel, W.J. Koros, Chain mobility, thermal, and mechanical properties of poly(ethylene furanoate) compared to poly(ethylene terephthalate), Macromolecules 47 (2014) 1383–1391, https://doi.org/10.1021/ma5000199.
[57] A. Bourdet, A. Esposito, S. Thiyagarajan, L. Delbreilh, F. Affouard, R.J.I. Knoop, E. Dargent, Molecular mobility in amorphous biobased poly(ethylene 2,5-furandicarboxylate) and poly(ethylene 2,4-furandicarboxylate), Macromolecules 51 (2018) 1937–1945, https://doi.org/10.1021/acs.macromol.8b00108.
[58] M. Manfroni, A. Coatti, M. Soccio, V. Siracusa, E. Boanini, E. Salatelli, N. Lotti, Eco-design of biobased poly(butylene succinate-b-pentamethylene 2,5-furanoate) copolymers with optimized mechanical, thermal and barrier properties for flexible food-packaging, Eur. Polym. J. 225 (2025) 113728, https://doi.org/10.1016/j.eurpolymj.2025.113728.
[59] M. Schmid, W. Zillinger, K. Muller, S. Sangerlaub, Permeation of water vapour, nitrogen, oxygen and carbon dioxide through whey protein isolated based films and coatings—Permselectivity and activation energy, Food Packag. Shelf. Life 6 (2015) 21–29, https://doi.org/10.1016/j.fpsl.2015.08.002.
[60] M.S. Hedenqvist, Barrier Packaging Materials, in: M. Kutz (Ed.), Handbook of Environmental Degradation of Materials, Elsevier, 2012. Second Edition883-862.
[61] G. Guidotti, M. Soccio, N. Lotti, M. Gazzano, V. Siracusa, A. Munari, Poly (propylene 2,5-thiophenedicarboxylate) vs. Poly(propylene 2,5-furandicarboxylate): two examples of high gas barrier bio-based polyesters, Polymers 10 (2018) 785, https://doi.org/10.3390/polym10070785.
[62] L. Genovese, M. Gigli, N. Lotti, M. Gazzano, V. Siracusa, A. Munari, M. Dalla Rosa, Biodegradable long chain aliphatic polyesters containing ether-linkages: synthesis, solid-State, and barrier properties, Ind. Eng. Chem. Res. 53 (2014) 10965–10973, https://doi.org/10.1021/ie5017865.
[63] G.L. Robertson, Chapter 4: optical, mechanical and barrier properties of thermoplastics polymers, in: G.L. Robertson (Ed.), Food Packaging-Principles and Practice, Taylor & Francis Group, 2013, pp. 91–130. Third Edition.
[64] Y. Tokiwa, B.P. Calabia, Biodegradability and biodegradation of polyesters, J. Polym. Environ. 15 (2007) 259–267, https://doi.org/10.1007/s10924-007-0066-3.
[65] M. Gigli, F. Quartinello, M. Soccio, A. Pellis, N. Lotti, G.M. Guebitz, S. Licoccia, A. Munari, Enzymatic hydrolysis of poly(1,4-Butylene 2,5-Thiophenedicarboxylate) (PBTF) and poly(1,4-Butylene 2,5-Furandicarboxylate) (PBF) films: a comparison of mechanisms, Environ. Int. 130 (2019) 104852, https://doi.org/10.1016/j.envint.2019.05.046.